

Black hole spin measurements through the relativistic precession model: XTE J1550-564

S.E. Motta¹, T. Muñoz-Darias², A. Sanna³, R. Fender², T. Belloni⁴, L. Stella⁵

¹ESAC, European Space Astronomy Centre, Villanueva de la Cañada, E-28692 Madrid, Spain

²University of Oxford, Department of Physics, Astrophysics, Denys Wilkinson Building, Keble Road, OX1 3RH, Oxford, United Kingdom ³Dipartimento di Fisica, Università degli

⁴INAF-Osservatorio Astronomico di Brera, Via E. Bianchi 46, I-23807 Merate, Italy

⁵INAF-Osservatorio Astronomico di Roma, Via Frascati 33, I-00040, Monteporzio Catone, Italy

3 September 2018

ABSTRACT

We present a systematic analysis of the complete set of observations of the black hole (BH) binary XTE J1550-564 obtained by the *Rossi X-ray Timing Explorer*. We study the fast time variability properties of the source and determine the spin of the black hole through the relativistic precession model. Similarly to what is observed in the BH binary GRO J1655-40, the frequencies of the QPOs and broad band noise components match the general relativistic frequencies of particle motion close to the compact object predicted by the relativistic precession model. The combination of two simultaneously observed quasi-periodic oscillation (QPO) frequencies together with the dynamical BH mass from optical/infrared observations yields a spin equal to $a = 0.34 \pm 0.01$, consistent with previous determinations from X-ray spectroscopy. Based on the derived BH parameters, the low frequency QPO emission radii vary from ~ 30 gravitational radii (R_g) to the innermost stable orbit for this spin ($\sim 5 R_g$), where they sharply disappear as observed for the case of GRO J1655-40.

Key words: Black hole - accretion disks - binaries: close - stars: individual: XTE J1550-564 - X-rays: stars

1 INTRODUCTION

Quasi periodic oscillations (QPOs) are commonly observed in the light curves from accreting compact objects and are thought to arise from the innermost regions of the accretion flow. In a power density spectrum (PDS) they take the form of relatively narrow peaks yielding accurate centroid frequencies that can be associated with dynamical motion and/or accretion related timescales in the presence of a gravitational field. Even though QPOs have been known for several decades and several authors proposed models to describe their origin [some of them involving the predictions of the Theory of General Relativity (GR), e.g. Esin et al. 1997, Titarchuk & Osherovich 1999, Tagger & Pellat 1999, Stella & Vietri 1998, Lamb & Miller 2001, Abramowicz & Kluźniak 2001, Ingram & Done 2011 and references therein], there is no consensus about their nature.

In black-hole systems, low-frequency (~ 0.1 – 30 Hz) QPOs (LFQPOs) of different kinds (dubbed type-A, -B and -C QPOs, see e.g. Casella et al. 2005 and Motta et al. 2011) have been detected. They usually show varying centroid frequencies and are often associated with broader peaked noise components (at ~ 1 – 100 Hz, see e.g. Belloni et al. 2011 for a review). QPOs with even higher frequencies (up to 450 Hz, high-frequency QPOs, HFQPOs) have also been detected (see, e.g. Strohmayer 2001), but only in a much smaller number of observations and sources. (Belloni et al. 2012).

They are usually divided into two classes, known as lower and upper HFQPOs.

Bound orbits of matter in a gravitational field are characterized by three different frequencies: the orbital frequency and the vertical and radial epicyclic frequencies. GR predicts that the motion of matter within a few tens of gravitational radii ($R_g = GM/c^2$) from black holes (BHs) carries the signatures of strong-field gravity effects. QPOs may provide the most promising prospects to measure such characteristic frequencies in the electromagnetic radiation emitted by the matter accreting onto a compact object. The relativistic precession model (RPM, Stella & Vietri 1998, Stella et al. 1999, Stella & Vietri 1999a, Motta et al. 2013) associates three different QPOs to a combination of the fundamental frequencies of particle motion. Type-C QPOs are associated with the nodal precession frequency (or Lense-Thirring frequency), while the periastron precession frequency and the orbital frequency correspond to the lower and upper HFQPOs, respectively. Motta et al. (2013) applied the RPM to data of the BH binary GRO J1655-40 and showed that it provides a natural interpretation for the QPOs and broad noise components observed in the PDS of the source. Motta et al. (2013) also showed that the RPM constitutes an effective tool to precisely determine both the mass and the spin of a black hole at the same time. Here, we use the same method to measure the spin of the BH binary XTE J1550-564, for which the dynamical mass has been re-

Table 1. Parameters of the simultaneous QPOs detected in the PDS from Obs. 30191-01-02-00 and used in this study. Note that a type B QPO is also present in the PDS.

QPO type	Frequency [Hz]	Width [Hz]	Normalization <i>Leahy</i>
type-B	4.92 ^{+0.03} _{-0.02}	0.33 ^{+0.09} _{-0.09}	0.57 ^{+0.03} _{-0.02}
type-C	13.08 ± 0.08	5.20 ^{+0.27} _{-0.26}	8.08 ^{+0.03} _{-0.02}
High-frequency	183 ± 5	84 ⁺²² ₋₁₇	6.1 ^{+1.0} _{-0.9}

cently measured through optical and infrared (OIR) observations. (Orosz et al. 2011).

2 OBSERVATIONS AND DATA ANALYSIS

We examined a total of 361 Rossi X-Ray Timing Explorer (RXTE)/Proportional Counter Array (PCA) archival observations¹ of XTE J1550-564 obtained between 1998 September 7 (MJD 51063) and 2004 June 6 (MJD 53162). The PCA data modes employed for most of these observations include a single-bit mode covering the absolute channel range 0–35 and a high-time-resolution event mode recording events above PCA absolute channel 36. For each observation we computed PDS using custom software under IDL (GHATS²) following the same method and extractions parameters described in Motta et al. (2013). We produced PDS in the 1.51–27.40 keV, 1.51–9.52 keV and 9.52–27.40 keV energy bands (corresponding to absolute channels 0–102, 0–35 and 36–102 at the beginning of the RXTE mission), to which we refer as total, soft and hard energy band. We used 64 and 128 seconds-long intervals of the event files and a Nyquist frequency of 2048 Hz to produce the PDS. Then, we averaged the individual PDS (obtaining a single PDS for each observation) and subtracted the contribution due to Poissonian noise (see Zhang et al. 1995). The PDS were normalized according to Leahy et al. (1983) and converted to square fractional rms (Belloni & Hasinger 1990). We measured the integrated fractional rms (defined as the rms integrated over a certain frequency band) in the 2–27 keV integrating the PDS over the 0.1–64 Hz frequency band and taking the square root of the power obtained (Muñoz-Darias et al. 2011).

PDS fitting was carried out with the XSPEC package by using a one-to-one energy-frequency conversion and an unit response. Following Belloni et al. (2002), we fitted the noise components with a number of broad Lorentzian shapes and both low frequency and high-frequency QPOs with a narrow Lorentzian. In the case of LFQPOs we added a variable number of Lorentzians depending on the presence of harmonic peaks. We measured the frequencies of the narrow features using the PDS produced from 64s-long intervals (because of their higher signal-to-noise), whereas the PDS from 128s long intervals were used for the broader components since they provide a lower minimum observable frequency.

Based on the results of the fitting, we excluded from the analysis non-significantly detected features (significances³ $\leq 3\sigma$,

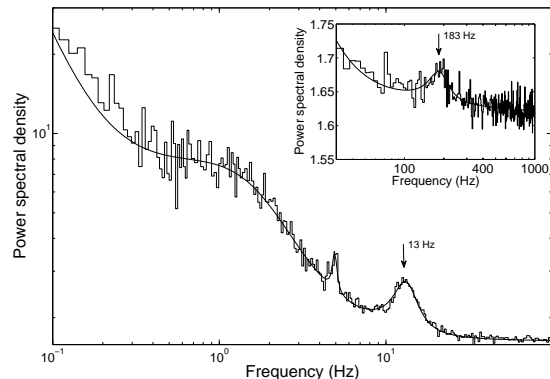


Figure 1. PDS obtained from Obs. 30191-01-02-00. The two simultaneously detected QPOs are marked (see large panel for the type-C QPO and the inset for the HFQPO). A narrow type-B QPO is also visible at ~ 5 Hz

Boutelier et al. 2010). The best fit parameters from all the observations that were considered are listed in Tab. 3.

2.1 QPO classification and sample selection

Type-C QPOs represent the BH equivalent of the so-called Horizontal Branch Oscillations (HBOs) observed in accreting neutron stars (Casella et al. 2005, but see Altamirano et al. 2012 for the case of HBOs in Terzan 5 X-2). Therefore Type C QPO are suited to be used in the framework of the RPM (Motta et al. 2013). Following Motta et al. (2012), we selected 49 observations showing type-C QPOs covering the 0.1–18 Hz frequency range (see Tab. 3). Among this sample, we searched for narrow features at high frequencies (> 100 Hz). We found only one observation that showed a HFQPO simultaneously to a type-C QPO (Obs Id 30191-01-02-00), both observable in the PDS of the total (see Fig. 1), soft and hard energy band. Non-simultaneous HFQPOs at ~ 180 Hz and ~ 280 Hz have been observed in XTE J1550-564 by Remillard et al. (1999) and Miller et al. (2001), later also reported by Belloni et al. (2012), who performed a systematic analysis of high-frequency QPOs in a sample of BH binaries. Miller et al. (2001) reported the simultaneous detection of two HFQPOs (at ~ 270 Hz and ~ 170 Hz, respectively), but unfortunately the latter was statistically not significant (Belloni et al. 2012). Méndez et al. (2013) systematically studied the phase lags of all the HFQPOs detected in XTEJ1550-564 and found that they correspond to a single lower HFQPO that changes frequency over time and that is observed between ~ 180 and ~ 280 Hz. Based on this work, we treated the peak at ~ 183 as a lower HFQPO. Observation 30191-01-02-00 also shows a peak at ~ 5 Hz that we classified as a type-B QPO. The two QPOs were classified based on the relation between rms and QPO centroid frequency, following the steps detailed in Motta et al. 2012. This is the second case in which simultaneous type-C and type-B QPOs are reported (see Motta et al. 2012 for GRO J1655-40). The parameters of the QPOs in Obs. 30191-01-02-00 are reported in Tab. 1.

3 RESULTS

3.1 From the Relativistic precession model to the spin measurement

The functional form of the RPM equations depends solely on the BH mass and spin and the radius at which the QPOs are produced.

¹ <http://heasarc.gsfc.nasa.gov/docs/xte/archive.html>

² http://www.brera.inaf.it/utenti/belloni/GHATS_Package/Home.html

³ The single trial significances of QPOs are given as the ratio of the integral of the power of the Lorentzian used to fit the QPO divided by the negative 1-sigma error on the integral of the power.

Table 2. Black hole parameters and associated quantities as measured from the RPM. For details, see the text, Sec. 3.1. *The BH mass is taken from the literature and it comes from Optical-Infrared dynamical studies (Orosz et al. 2011).

	Mean value	Standard deviation
Mass* (Solar masses)	9.1	0.6
Spin	0.341	0.007
Radius (Gravitational radii)	5.47	0.12
R_{ISCO} (Gravitational radii)	4.83	0.02
ν_{nod} at R_{ISCO} (Hz)	18	1

The system of equations can be solved whenever the three QPOs are observed simultaneously. This condition is not satisfied for XTE J1550-564, where only a type-C QPO and a HFQPO are simultaneously detected. However, if we use the BH mass as recently determined from optical spectro-photometric observations ($M = 9.10 \pm 0.61 M_{\odot}$, Orosz et al. 2011), the emission radius and BH spin remain the only unknowns in the application of the RPM to the QPOs of XTE J1550-564 and the model equations can thus be solved. We proceeded as follows:

(i) For the nodal and the periastron precession frequencies (ν_{per} and ν_{nod} in eq. 7, Motta et al. 2013) we used the Newton-Raphson method to calculate the set of radii at which the observed frequencies (type-C QPO and lower HFQPO, respectively) are produced for every possible combination of mass and spin in a given range. We considered masses between 3 and 50 M_{\odot} with a resolution of 0.01 M_{\odot} and spins between 0 and 1 with a resolution of 0.001. This results in two independent sets of mass-spin-radius solutions.

(ii) We inferred the spin that for a mass fixed at the OIR value, solves simultaneously the two equations equations of step (i).

(iii) Through the Monte-Carlo method we simulated 10^5 sets of two frequencies and BH mass. The distributions are Gaussian, centred at the mean value and with a width equal to the error on the centroid frequencies and the mass, respectively.

(iv) We solved the RPM system following step 1 and 2. As a result we obtained two distributions of spins and emission radii consistent with being Gaussian-distributed.

(v) Fitting the distribution of spin and radius from step (iv), we obtained the following measurements: spin $a/M = 0.341 \pm 0.007$, radius $= (5.47 \pm 0.12) R_g$. The best fit parameters are shown in Tab. 2.

(vi) From the spin and the BH mass distributions we obtained a distribution of values for R_{ISCO} (see Motta et al. 2013) and its corresponding nodal frequency. We find $R_{\text{ISCO}} = (4.83 \pm 0.02) R_g$ for XTE J1550-564.

3.2 The PBK correlation and the distribution of the type-C QPOs

In the PDS of BHs and NSs X-ray binaries, the frequency of two power-spectral components follow a tight correlation over a very large frequency range (Psaltis et al. 1999). This correlation involves either two QPOs (a low-frequency QPO and either the lower or the upper HFQPO) or a LFQPO and a broad noise component. Following Stella et al. (1999) and Motta et al. (2013), we inspected the observations of our sample to identify the power-spectral compo-

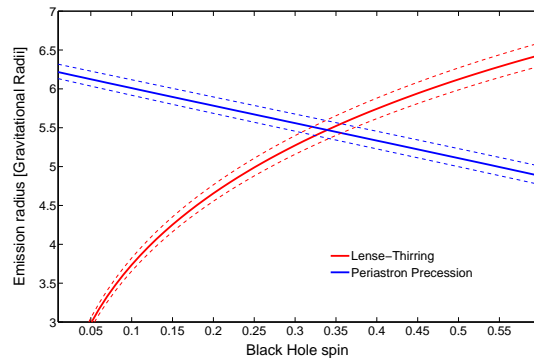


Figure 2. Spin as a function of the emission radius as predicted by the two relevant equations of the relativistic precession model (blue line for nodal precession frequency; red line for periastron precession frequency) for the black hole binary XTE J1550-564. The derived black hole spin is $a = 0.34 \pm 0.01$. The solid line marks the measured values and the dashed lines mark the 1-sigma confidence level. For the latter, only the error in the BH mass (which is dominant) is considered.

nent following the PBK correlation (L_{lf} , L_l and L_u according to Belloni et al. 2002).

We considered the characteristic frequency ν_{max}^4 of the components L_l and L_u and the centroid frequency L_{lf} of the type-C QPO (Motta et al. 2013). We plotted the characteristic frequencies L_l and L_u as a function of the LFQPO centroid frequency. We also plotted the frequencies predicted by the RPM using the OIR mass and the spin and emission radius obtained in Sec. 3.1. The result is shown in Fig. 3.

- The characteristic frequencies of the L_l and L_u components follow fairly closely the frequencies predicted by the RPM. The L_l frequencies approximately match the periastron precession frequency, while the L_u frequencies follow the orbital frequency (see Fig. 3). Most L_l and L_u components centroid frequencies are consistent within 3σ with the frequencies predicted by the RPM. Only two points are marginally consistent.

- Type C QPOs are observed to vary over a broad frequency range. All of them are consistent with being produced at radii larger than R_{ISCO} . The highest frequency Type-C QPO is centred at 18.04 Hz, which would correspond to a radius equal to 4.9 gravitational radii, only $\sim 1.6\%$ larger than R_{ISCO} .

3.3 On the width of the QPOs

The QPOs observed in BH X-ray binaries are typically narrow, with very small fractional widths (van der Klis 1997), which provide an indication on the geometrical structure of the region where they are produced. As noted by Motta et al. (2013), the simplest assumption we can make is that the QPOs are produced in a narrow annulus in the accretion flow. To obtain a rough estimate of the radial size of this annulus, we apply a variable jitter dr to the emission radius at which the QPOs are produced. Following Motta et al. (2013) we started with a very small jitter and we increased dr until we obtained a distribution of RPM frequencies with FWHM consistent with the FWHM of the observed QPOs. We see that a jitter between 5.3% and 5.7% of the emission radius is able to reproduce

⁴ ν_{max} is defined as $(\nu_{\text{max}}^2 = \nu^2 + (\Delta/2)^2)$, where Δ is the width of the Lorentzian component describing a given power-spectral feature (Belloni et al. 2002).

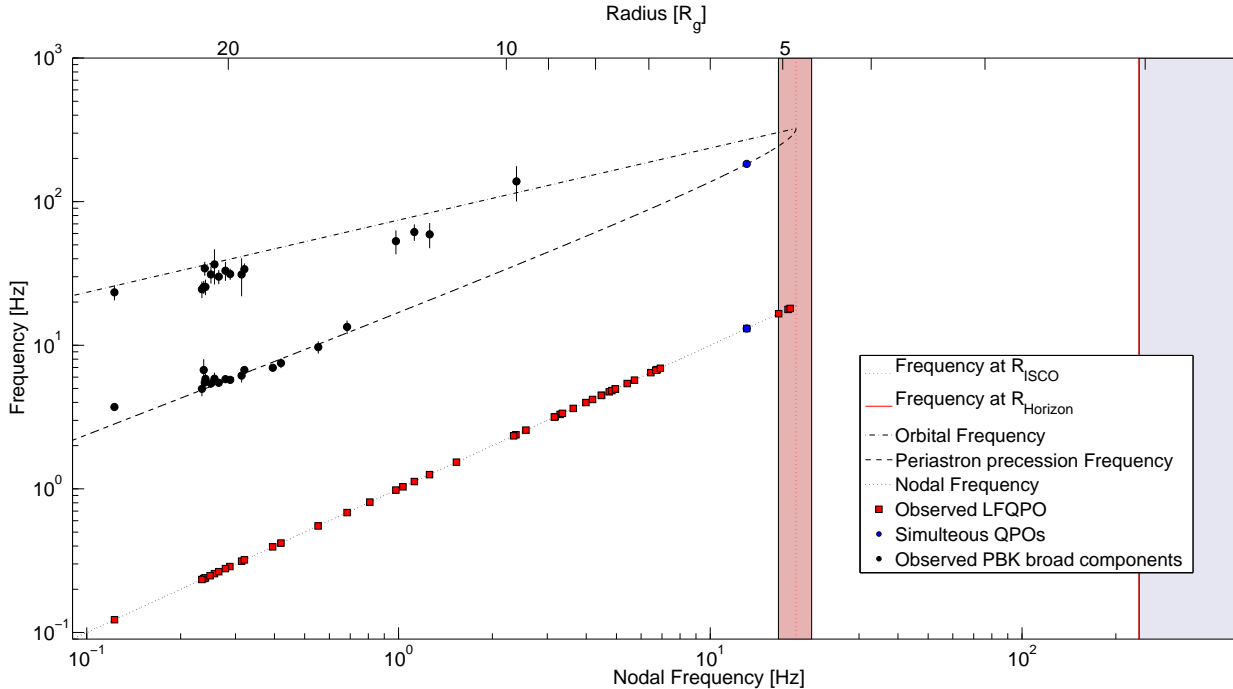


Figure 3. Nodal frequency (dotted line), periastron precession frequency (dashed line) and orbital frequency (dot-dashed line) as a function of the nodal precession frequency around a Kerr black hole as predicted by the relativistic precession model for QPOs. The lines are drawn for mass $M = 9.10 M_{\odot}$ and spin $a/M = 0.34$. The corresponding radii are given in the top X-axis. The blue points, the black circles and the red squares represent the simultaneous lower HFQPO and type-C QPO, the characteristic frequencies of the broad components following the PBK correlation and the type-C QPOs frequencies plotted against itself, respectively. The vertical dotted red line marks the nodal frequency produced at the innermost stable circular orbit and the red vertical band indicates its corresponding 3-sigma uncertainty.

the widths of the two simultaneous QPOs observed in XTE J1550-564.

4 DISCUSSION

We have examined 361 RXTE archival observations of the BH binary XTE J1550-564 from its 1998 and 2000 outburst and in one case we simultaneously detected a type-C QPO and a HFQPO. Following Motta et al. (2013), we applied the RPM to XTE J1550-564 by combining the centroid frequencies of the QPOs together with the BH mass inferred from OIR observations. We obtained a spin of $a/M = 0.34 \pm 0.01$ and an emission radius for the QPOs of $(5.5 \pm 0.1)R_g$. Assuming that the two simultaneous QPOs (Type-C and lower HFQPO) arise from an annular region around the emission radius, assuming a jitter of the emission radius we estimate the width of this annulus to be $\pm 5 - 6\%$ of the emission radius. This is in agreement with the results by Heil et al. (2011), who showed that the Type-C QPOs in XTE J1550-564 display frequency jitter on short timescales (seconds) and also reported that the frequency of the Type-C QPO correlates with the flux over these timescales. This quantitatively supports our treatment of the radius jitter since for larger radii (R+dr) we expect lower QPO frequencies and fluxes than for smaller radii (R-dr).

As a check, we also solved the RPM system assuming that the HFQPO at ~ 183 Hz corresponds to the orbital frequency (instead of the periastron precession frequency). We obtained a spin of $a/M = 0.84$ and an emission radius of $7R_g$. We plotted the frequencies predicted by the RPM using these values and the characteristic frequencies L_l and L_u (see Sec. 3.2), but we found that

there is no agreement between the observed and the predicted frequencies. Therefore, we can exclude that the HFQPO at ~ 183 Hz corresponds to the orbital frequency.

Steiner et al. (2011) reported a measurement of the spin of the BH in XTE J1550-564 by modelling both the thermal continuum spectrum of the accretion disc and by fitting the Fe-K α line. They obtained $-0.11 < a/M < 0.71$ (90 per cent confidence) for the former method, whereas the latter results in $a/M = 0.55^{+0.15}_{-0.22}$. Their combined result is $a/M = 0.49^{+0.13}_{-0.20}$, consistent with the value reported in this work.

In Motta et al. (2013) we found that the spin value from the RPM to the data of GRO J1655-40 disagreed with the value obtained from both the thermal continuum modelling and the Fe-K α line fitting. However, we note that despite the fact that the orbital inclination of GRO J1655-40 and XTE J1550-564 are comparable (both have been estimated between 70 and 75 degrees, Orosz et al. 2002, Greene et al. 2001), Greene et al. (2001) found that in GRO J1655-40 the jet axis - which is presumably aligned with the BH spin axis - and the orbital axis are misaligned by $> 15^\circ$. On the contrary, Steiner & McClintock (2012) determined the inclination angle of the jet axis in XTE J1550-564 and found that it is probably aligned with the BH spin axis (they infer an upper limit to the BH spin-jet axis misalignment of 12°). Therefore, while the assumption that the spin inclination to the line of sight is the same as the orbital inclination seems correct within small errors in the case of XTE J1550-564, this might not be true for GRO J1655-40. In any case, it is clear that more timing measurements are needed to test whether the RPM-based method and the two spectroscopic methods are generally consistent [note that in some cases the spectroscopic methods already disagree (Reynolds 2013)]. However, since currently

available data do not provide the adequate signal to noise to further probe this apparent inconsistency, it is clear that only new generation satellites such as LOFT (Feroci & LOFT Consortium 2011) will be able to tell us more about HF QPOs and to solve the issue.

The spin value obtained from the RPM, together with the mass estimated from the OIR allow us to predict the expected behaviour of the frequencies for each QPO type in XTE J1550-564. All frequencies reach their highest theoretically allowed values at the innermost stable circular orbit, where the relativistic effective potential has an inflection point and the orbital and periastron precession frequencies coincide (at ~ 320 Hz). Based on the mass and spin values that we measure, the ISCO is expected at a radius of $4.8 R_g$, corresponding to a nodal precession frequency of 18.8 Hz.

Once the RPM is solved, the identification of any of the three frequencies relevant to the RPM at other times allows us to measure the corresponding emission radius. In many of the RXTE observations, XTE J1550-564 displayed low-frequency QPOs (Fig. 3) whose frequency varied over a wide range, covering about two decades, from ~ 0.1 Hz to ~ 18 Hz (Motta et al. 2012). The lowest frequency type-C QPO is produced at ~ 30 gravitational radii from the BH, while the highest arises from a radius consistent with the ISCO radius. A similar result was found for the case of GRO J1655-40.

As already noted by Stella & Vietri (1999a), the RPM also provides a natural interpretation for the PBK correlation (Psaltis et al. 1999), which involves either two QPOs (a low-frequency QPO and either the lower or the upper HFQPO) or a low-frequency QPO and a broad noise component. Following Motta et al. (2013), the periastron precession and orbital frequencies as a function of the nodal frequency match the correlation between the type-C QPOs and the broad noise components frequencies observed in GRO J1655-40 (see Fig. 3). Differently from what we saw in GRO J1655-40, in XTE J1550-564 we simultaneously observe the L_l and the L_u components (associated to the periastron precession and to the orbital motion, respectively, in the RPM framework). We note that, in general, the centroid frequencies of the L_l and the L_u components display some scatter around the RPM predicted frequencies. Furthermore, the L_u characteristic frequencies tend to be shifted to lower frequencies than the predicted frequencies. We identify three different reasons for this:

- Deviations of the behaviour of the matter in the accretion flow from the test-particle description are expected especially at large radii (i.e. when the type-C QPO shows a centroid frequency below ~ 1), when the region in which both QPOs and broad frequencies originate is probably radially larger than at smaller radii.
- Differently from QPOs (which are relatively narrow), the precision with which the characteristic frequencies of the broad PBK components are measured is affected by the model used to fit them. This introduces additional uncertainties that could partly explain the scatter/shift of the points and their relative shift. However, a detailed treatment of these uncertainties is beyond the scope of this work and it will be discussed in a forthcoming paper (Motta et al. in prep).
- The point above is particularly true for the L_u component, which is the hardest to constrain. In general, disentangling the L_l and the L_u components is problematic and constraining well the parameters is often prevented by the low S/N at high frequencies (above ~ 10 Hz, where these broad components are more powerful).

5 SUMMARY AND CONCLUSIONS

XTE J1550-564 is the second black hole binary whose timing properties can be interpreted in terms of motion of matter in the close vicinity of a rotating BH. Here, we report a spin measurement for the BH in this source obtained by applying the relativistic precession model and based on the method presented in Motta et al. (2013). We combine the results from X-ray timing (i.e. the frequency of two different simultaneously observed oscillations) with the dynamical BH mass obtained from OIR observations, yielding spin and emission radius measurements with formal errors as small as $\sim 2\%$ ($a/M = 0.34 \pm 0.01$), the former being consistent with previous results obtained through X-ray spectroscopy.

The agreement between the predictions of the RPM and the actual timing properties of XTE J1550-564 strengthen the conclusions reported by Motta et al. (2013) and further supports the hypothesis that both the QPOs and broad noise components in accreting BH binaries could, on average, be explained in terms of motion of matter in the close vicinity (a few tens R_g down to a few R_g) of a BH.

The authors acknowledge the anonymous referee for his/her helpful comments and suggestions that contributed to improve this work. SEM acknowledges the ESA research fellowship program. SEM also acknowledges Jiri Svoboda for useful discussions. TMD acknowledges funding via an EU Marie Curie Intra-European Fellowship under contract no. 2011-301355. SM and TMB acknowledge support from INAF PRIN 2012-6 This research has made use of data obtained from the High Energy Astrophysics Science Archive Research Center (HEASARC), provided by NASA's Goddard Space Flight Center.

REFERENCES

- Abramowicz M. A., Kluźniak W., 2001, *A&A*, 374, L19
 Altamirano D., Ingram A., van der Klis M., Wijnands R., Linares M., Homan J., 2012, *ApJ*, 759, L20
 Belloni T., Hasinger G., 1990, *A&A*, 230, 103
 Belloni T., Psaltis D., van der Klis M., 2002, *ApJ*, 572, 392
 Belloni T. M., Motta S. E., Muñoz-Darias T., 2011, *Bulletin of the Astronomical Society of India*, 39, 409
 Belloni T. M., Sanna A., Méndez M., 2012, *MNRAS*, 426, 1701
 Boutelier M., Barret D., Lin Y., Török G., 2010, *MNRAS*, 401, 1290
 Casella P., Belloni T., Stella L., 2005, *ApJ*, 629, 403
 Esin A. A., McClintock J. E., Narayan R., 1997, *ApJ*, 489, 865
 Feroci M., LOFT Consortium t., 2011, *ArXiv e-prints*
 Greene J., Bailyn C. D., Orosz J. A., 2001, *ApJ*, 554, 1290
 Heil L. M., Vaughan S., Uttley P., 2011, *MNRAS*, 411, L66
 Ingram A., Done C., 2011, *MNRAS*, 415, 2323
 Lamb F. K., Miller M. C., 2001, *ApJ*, 554, 1210
 Leahy D. A., Elsner R. F., Weisskopf M. C., 1983, *ApJ*, 272, 256
 Méndez M., Altamirano D., Belloni T., Sanna A., 2013, *MNRAS*
 Miller J. M., Wijnands R., Homan J., Belloni T., Pooley D., Corbel S., Kouveliotou C., van der Klis M., Lewin W. H. G., 2001, *ApJ*, 563, 928
 Motta S., Homan J., Muñoz Darias T., Casella P., Belloni T. M., Hiemstra B., Méndez M., 2012, *MNRAS*, 427, 595
 Motta S., Muñoz-Darias T., Casella P., Belloni T., Homan J., 2011, *MNRAS*, 418, 2292
 Motta S. E., Belloni T. M., Stella L., Muñoz-Darias T., Fender R., 2013, *ArXiv e-prints*

- Muñoz-Darias T., Motta S., Belloni T. M., 2011, MNRAS, 410, 679
- Orosz J. A., Groot P. J., van der Klis M., McClintock J. E., Garcia M. R., Zhao P., Jain R. K., Bailyn C. D., Remillard R. A., 2002, ApJ, 568, 845
- Orosz J. A., Steiner J. F., McClintock J. E., Torres M. A. P., Remillard R. A., Bailyn C. D., Miller J. M., 2011, ApJ, 730, 75
- Psaltis D., Belloni T., van der Klis M., 1999, ApJ, 520, 262
- Remillard R. A., McClintock J. E., Sobczak G. J., Bailyn C. D., Orosz J. A., Morgan E. H., Levine A. M., 1999, ArXiv Astrophysics e-prints
- Reynolds C. S., 2013, Space Science Reviews
- Steiner J. F., McClintock J. E., 2012, ApJ, 745, 136
- Steiner J. F., Reis R. C., McClintock J. E., Narayan R., Remillard R. A., Orosz J. A., Gou L., Fabian A. C., Torres M. A. P., 2011, MNRAS, 416, 941
- Stella L., Vietri M., 1998, ApJ, 492, L59+
- Stella L., Vietri M., 1999a, Physical Review Letters, 82, 17
- Stella L., Vietri M., Morsink S. M., 1999, ApJ, 524, L63
- Strohmayer T. E., 2001, ApJ, 552, L49
- Tagger M., Pellat R., 1999, A&A, 349, 1003
- Titarchuk L., Osherovich V., 1999, ApJ, 518, L95
- van der Klis M., 1997, Advances in Space Research, 19, 75
- Zhang W., Jahoda K., Swank J. H., Morgan E. H., Giles A. B., 1995, ApJ, 449, 930

Table 3: Observations included in our sample. We report the Observation Id, the time at which the observation was taken, the integrated fractional rms (measured in the 2-27 keV energy band and in the 0.0-64.0 Hz frequency range), the hardness ratio calculated as described in Sec. 2, the centroid frequency of the Type-C QPO observed, the characteristic frequency (ν_{Max}) of the broad high-frequency component - when detected. For details on the model used to fit the PDS, see Sec. 2

				Type-C QPOs	broad component L_l	broad component L_u
Time [<i>MJD</i>]	Obs. ID	Hardness ratio	rms [%]	ν [<i>Hz</i>]	ν_{Max} [<i>Hz</i>]	ν_{Max} [<i>Hz</i>]
51065.1	30188-06-01-00	0.948 ± 0.003	31.0 ± 0.3	0.288 ^{+0.001} _{-0.001}	3.7 ^{+0.1} _{-0.1}	23 ⁺³ ₋₃
51065.3	30188-06-01-01	0.937 ± 0.003	28.5 ± 0.3	0.395 ^{+0.002} _{-0.002}	5.7 ^{+0.3} _{-0.3}	31 ⁺² ₋₃
51066.1	30188-06-01-02	0.892 ± 0.003	26.2 ± 0.2	0.809 ^{+0.002} _{-0.002}	7.0 ^{+0.3} _{-0.3}	-
51066.3	30188-06-01-03	0.865 ± 0.003	26.5 ± 0.2	1.034 ^{+0.003} _{-0.003}	9.1 ^{+0.5} _{-0.5}	-
51064.0	30188-06-03-00	0.968 ± 0.003	32.1 ± 0.3	0.123 ^{+0.001} _{-0.001}	-	-
51067.3	30188-06-04-00	0.798 ± 0.002	26.5 ± 0.2	1.534 ^{+0.004} _{-0.004}	-	-
51068.3	30188-06-05-00	0.701 ± 0.002	23.4 ± 0.2	2.381 ^{+0.005} _{-0.005}	-	138 ⁺⁴⁷ ₋₃₈
51069.3	30188-06-06-00	0.623 ± 0.002	20.6 ± 0.1	3.297 ^{+0.006} _{-0.006}	-	-
51070.1	30188-06-07-00	0.632 ± 0.002	20.9 ± 0.1	3.182 ^{+0.004} _{-0.004}	-	-
51070.3	30188-06-08-00	0.634 ± 0.002	20.8 ± 0.1	3.161 ^{+0.004} _{-0.003}	-	-
51071.2	30188-06-09-00	0.601 ± 0.002	20.0 ± 0.1	3.634 ^{+0.005} _{-0.005}	-	-
51072.0	30188-06-10-00	0.680 ± 0.002	22.3 ± 0.3	2.563 ^{+0.006} _{-0.006}	-	-
51072.3	30188-06-11-00	0.585 ± 0.002	19.3 ± 0.1	3.992 ^{+0.005} _{-0.005}	-	-
51074.1	30191-01-01-00	0.533 ± 0.002	16.2 ± 0.1	5.713 ^{+0.010} _{-0.010}	-	-
51076.0	30191-01-02-00	0.600 ± 0.002	2.5 ± 0.0	13.087 ^{+0.080} _{-0.080}	-	-
51087.7	30191-01-18-01	0.621 ± 0.002	22.5 ± 0.2	3.356 ^{+0.008} _{-0.008}	-	-
51096.6	30191-01-27-00	0.538 ± 0.002	18.5 ± 0.1	5.414 ^{+0.009} _{-0.009}	-	-
51095.6	30191-01-27-01	0.573 ± 0.002	20.8 ± 0.2	4.481 ^{+0.009} _{-0.009}	-	-
51097.8	30191-01-28-00	0.586 ± 0.002	21.8 ± 0.2	4.191 ^{+0.010} _{-0.010}	-	-
51097.6	30191-01-28-01	0.561 ± 0.002	20.3 ± 0.1	4.742 ^{+0.009} _{-0.009}	-	-
51098.3	30191-01-28-02	0.558 ± 0.002	20.1 ± 0.1	4.959 ^{+0.009} _{-0.009}	-	-
51099.2	30191-01-29-00	0.559 ± 0.002	20.2 ± 0.1	4.835 ^{+0.009} _{-0.009}	-	-
51099.6	30191-01-29-01	0.557 ± 0.002	19.9 ± 0.1	4.961 ^{+0.007} _{-0.007}	-	-
51100.3	30191-01-30-00	0.513 ± 0.002	15.3 ± 0.1	6.449 ^{+0.009} _{-0.009}	-	-
51101.6	30191-01-31-00	0.504 ± 0.002	13.9 ± 0.1	6.764 ^{+0.020} _{-0.020}	-	-
51101.9	30191-01-31-01	0.507 ± 0.002	14.3 ± 0.1	6.718 ^{+0.012} _{-0.012}	-	-
51644.5	50137-02-01-00	0.801 ± 0.003	31.5 ± 0.2	0.237 ^{+0.002} _{-0.002}	6.7 ^{+1.1} _{-1.3}	25 ⁺⁴ ₋₃
51646.3	50137-02-02-00	0.795 ± 0.003	31.6 ± 0.3	0.257 ^{+0.003} _{-0.003}	5.8 ^{+0.6} _{-0.6}	37 ⁺¹² ₋₁₀
51646.6	50137-02-02-01	0.799 ± 0.003	31.5 ± 0.3	0.265 ^{+0.002} _{-0.002}	5.5 ^{+0.3} _{-0.3}	30 ⁺³ ₋₃
51648.7	50137-02-03-00	0.796 ± 0.003	32.4 ± 0.3	0.239 ^{+0.002} _{-0.002}	5.5 ^{+0.3} _{-0.3}	34 ⁺⁵ ₋₄
51649.8	50137-02-03-01G	0.803 ± 0.004	32.7 ± 0.4	0.240 ^{+0.002} _{-0.002}	5.8 ^{+0.5} _{-0.5}	25 ⁺³ ₋₃
51650.7	50137-02-04-00	0.796 ± 0.003	33.0 ± 0.3	0.234 ^{+0.003} _{-0.003}	5.0 ^{+0.6} _{-0.5}	25 ⁺⁶ ₋₃
51651.4	50137-02-04-01	0.792 ± 0.003	32.2 ± 0.2	0.249 ^{+0.002} _{-0.002}	5.4 ^{+0.3} _{-0.4}	31 ⁺⁴ ₋₄
51652.2	50137-02-05-00	0.795 ± 0.003	31.9 ± 0.3	0.279 ^{+0.003} _{-0.003}	5.8 ^{+0.3} _{-0.4}	33 ⁺⁴ ₋₅
51653.5	50137-02-05-01	0.787 ± 0.003	32.4 ± 0.3	0.314 ^{+0.002} _{-0.002}	6.1 ^{+0.7} _{-0.6}	31 ⁺⁷ ₋₉
51654.7	50137-02-06-00	0.784 ± 0.003	32.8 ± 0.3	0.320 ^{+0.002} _{-0.002}	6.7 ^{+0.4} _{-0.4}	34 ⁺³ ₋₃
51655.7	50137-02-07-00	0.777 ± 0.003	31.8 ± 0.5	0.420 ^{+0.003} _{-0.003}	7.5 ^{+0.5} _{-0.6}	-
51658.6	50134-02-01-00	0.712 ± 0.003	29.8 ± 0.4	1.257 ^{+0.006} _{-0.006}	-	59 ⁺¹³ ₋₁₂
51676.4	50134-01-04-00	0.443 ± 0.002	14.4 ± 0.1	6.915 ^{+0.022} _{-0.022}	-	-
51678.5	50134-01-05-00	0.550 ± 0.002	20.6 ± 0.1	4.476 ^{+0.011} _{-0.011}	-	-
51682.3	50135-01-02-00	0.669 ± 0.003	25.4 ± 0.2	2.340 ^{+0.010} _{-0.010}	-	-
51683.8	50135-01-03-00	0.736 ± 0.003	26.1 ± 0.1	1.124 ^{+0.007} _{-0.007}	-	61 ⁺⁹ ₋₈
51684.8	50135-01-04-00	0.750 ± 0.005	25.4 ± 0.3	0.981 ^{+0.020} _{-0.020}	-	53 ⁺¹⁰ ₋₁₀
51686.3	50135-01-05-00	0.761 ± 0.004	26.0 ± 0.2	0.684 ^{+0.008} _{-0.008}	13.4 ^{+1.6} _{-1.4}	-
51687.2	50135-01-06-00	0.772 ± 0.005	26.1 ± 0.3	0.552 ^{+0.009} _{-0.008}	9.7 ^{+1.3} _{-0.9}	-
51115.3	30191-01-36-00	0.361 ± 0.001	4.1 ± 0.1	16.576 ^{+0.201} _{-0.224}	-	-
51180.8	40401-01-02-00	0.304 ± 0.001	2.2 ± 0.0	17.766 ^{+0.118} _{-0.121}	-	-
51239.1	40401-01-48-00	0.291 ± 0.001	2.4 ± 0.0	18.037 ^{+0.069} _{-0.067}	-	-